Title Page

AAV-Mediated Rhodopsin Replacement Provides Therapeutic Benefit in Mice with a Targeted Disruption of the Rhodopsin Gene

Arpad Palfi[1,3,4], Sophia Millington-Ward[1,3], Naomi Chadderton[1], Mary O'Reilly[1], Tobias Goldmann[2], Marian M Humphries[1], Uwe Wolfrum[2], Peter Humphries[1], Paul F Kenna[1] and G Jane Farrar[1].

[1]Department of Genetics, Trinity College Dublin, Dublin 2, Ireland; [2]Institute of Zoology, Cell and Matrix Biology, Johannes Gutenberg University of Mainz, Mainz, Germany; [3]These authors contributed equally; [4]Corresponding author.

Corresponding Author:

Arpad Palfi

Department of Genetics

Trinity College Dublin

Dublin 2, Ireland

Phone: 353-1-8962484

Fax: 353-1-8963848

Email: palfia@tcd.ie

Running title:

Gene replacement in rhodopsin null mice

Abstract

The rhodopsin gene (*RHO*) encodes a highly expressed G protein-coupled receptor (GPCR) which is central to visual transduction in rod photoreceptors. A suite of recombinant 2/5 adeno-associated virus (AAV) *RHO* replacement vectors has been generated in an attempt to recapitulate endogenous rhodopsin levels from exogenously delivered AAV vectors in the retina of mice with a targeted disruption in the rhodopsin gene (*Rho*-/- mice). Approximately 40% of wild type mouse rhodopsin mRNA levels (RNA taken from whole retinas) were achieved *in vivo* in AAV-*RHO*-injected eyes, representing approximately 50-fold increases in expression comparative with the initial vector. The main focus of this study was to test whether expression of AAV-*RHO* replacement in *Rho*-/- mice provided therapeutic benefit, which to date had not been achieved. *Rho-/-* mice neither elaborate rod outer segments nor have rod-derived electroretinograms (ERG). Our results indicate for the first time in this model that subretinal AAV-*RHO* delivery leads not only to RHO immunolabelling but the generation of rod outer segments as evaluated by light and transmission electron microscopy. Improved histology was accompanied by rod photoreceptor activity as assessed by ERG for at least twelve weeks post-injection. The most efficient AAV-*RHO* constructs presented in this study provide sufficient levels of RHO to be of therapeutic benefit in *Rho-/-* mice and therefore represent important steps towards generating potent AAV-*RHO* replacement genes for gene therapy in *RHO*-linked human retinopathies.

Introduction

The rhodopsin protein, which represents the main component of the disc membranes of rod photoreceptor outer segments, participates in one of the most extensively studied G protein-coupled receptor (GPCR) mediated pathways, that of phototransduction (Palczewski, 2006). Interest in this highly expressed photoreceptor GPCR has been fuelled by seminal discoveries over the past three decades involving characterisation of the structure of the receptor, its ligand binding site and activation mechanisms amongst many others (Unger *et al*., 1997; Hamm *et al*., 1988). The distillation of information from a variety of disciplines provided the first functional characterisation of any molecule involved in mammalian vision. Additionally, it provided a template for future studies of different components of visual transduction and of various GPCRs of which there are approximately 1,000 (Palczewski, 2006).

The rhodopsin gene is highly expressed in rod photoreceptors, with the encoded transmembrane protein constituting approximately 90% of the total protein content of mammalian rod outer segment (ROS) disc membranes. Rhodopsin traverses the disc membranes at seven domains, typifying the structure of GCPRs. On average each ROS in the murine retina contains approximately 900 discs which are continually replaced at a rate of approximately 10% per day (Palczewski, 2006; Ludowski *et al*., 2009). The development of mice with disruptions of the endogenous mouse rhodopsin (*Rho*) gene (*Rho*-/- mice; Humphries *et al*., 1997; Lem *et al*. 1999) has provided a valuable tool for further exploration of rhodopsin. Homozygous *Rho*-/- mice do not elaborate ROS, have

no recordable rod photoreceptor electroretinogram (ERG) and lose photoreceptors over approximately a 3-4 month period post-natally; a timeframe of loss modulated somewhat by genetic background (Hobson *et al*., 2000).

A repertoire of recombinant viral vectors including lenti-, adeno- and adeno-associated viral (AAV) vectors mediate *in vivo* gene delivery to photoreceptor cells and can be used to explore gene therapies in animal models (Ledherz *et al*., 2008; Li *et al*., 2008; Surace *et al*., 2008; Stieger *et al*., 2009). In recent studies AAV serotypes including AAV2/5 and AAV2/8 have been predominantly used for gene delivery to photoreceptors due to efficient transduction, relatively low toxicity and the long term gene expression which can be achieved (Ledherz *et al*., 2008; Li *et al*., 2008; Surace *et al*., 2008; Stieger *et al*., 2009). The profile of AAV for retinal gene therapy has been further enhanced by results from recent Phase I human clinical trials supporting the safety of AAV2/2 in the human eye (Bainbridge *et al*., 2008; Cideciyan *et al*., 2008; Maguire *et al*., 2008).

Over the past two decades mutant rhodopsins have been implicated in a variety of inherited eye disorders (Farrar *et al*., 2002) including congenital stationary night blindness, autosomal dominant and autosomal recessive Retinitis Pigmentosa (RP) (www.sph.uth.tmc.edu/RetNet/). RP encompasses a group of genetic diseases which involves the progressive death of photoreceptor cells, frequently resulting in significant visual handicap (Bhatti, 2006). The human rhodopsin gene (*RHO*) was the first gene to be identified as causative of autosomal dominant RP (adRP) (McWilliam *et al*., 1989; Dryja *et al*., 1990; Farrar *et al*., 1990) and represents the most common gene implicated in

adRP, accounting for approximately 25% of cases (McWilliam *et al*., 1989; Dryja *et al*., 1990; Farrar *et al*., 1990; Farrar *et al*., 2002; www.sph.uth.tmc.edu/RetNet/). Over 100 mutations have been identified thus far, demonstrating that significant mutational heterogeneity exists in *RHO*-linked adRP.

Knowledge of the underlying genetic pathogenesis, together with the availability of animal models (Olsson *et al*., 1992; Li *et al*., 1996; Humphries *et al*., 1997) and vectors for delivery, has enabled exploration of gene-based therapies for inherited retinopathies. Many of these studies have focused on treatment of recessively inherited degenerations. For example AAV2/2-mediated delivery of the *RPE-65* gene to Briard dogs presenting with *RPE-65*-linked Leber congenital amaurosis (LCA) has been shown to restore vision (Acland *et al*., 2001). Currently, four human clinical trials for *RPE-65* associated LCA are either under way (Bainbridge *et al*., 2008; Cideciyan *et al*., 2008; Maguire *et al*., 2008) or should commence shortly (Le Meur *et al*., 2007). Therapeutic benefit in the recessive AIPL1 mouse model of LCA has also recently been demonstrated (Tan *et al*., 2009).

In contrast to recessive disease, progress in developing gene therapies for dominant retinal disorders such as *RHO*-linked adRP has been slower for a multiplicity of reasons. Since significant mutational heterogeneity is associated with *RHO*-linked adRP (www.sph.uth.tmc.edu/RetNet/), development of individual mutation-specific therapies has not been viable. To circumvent mutational heterogeneity, mutation-independent therapies involving suppression and replacement are being explored (Millington-Ward et

al., 1997; Lewin *et al*., 1998; LaVail *et al*., 2000; Cashman *et al*., 2005; Kiang *et al*., 2005; Palfi *et al*., 2006; Gorbatyuk *et al*., 2007; O'Reilly *et al*., 2007; Chadderton *et al*., 2009). Notably, RHO replacement is central to such an approach. Considering the high levels of endogenous RHO expression, a replacement *RHO* gene would need to be highly expressed to provide sufficient levels of protein for normal visual function. Adequate replacement is also an essential element of any combined suppression and replacement strategy. Given the physiological requirement for high levels of rhodopsin in mammalian rod photoreceptors, the primary focus of this study was to explore the optimisation of *RHO* replacement expression from AAV2/5 vectors in an attempt to achieve sufficient RHO levels to provide functional benefit in a murine model lacking endogenous rhodospin, a challenging task (*Rho*-/- mice; Humphries *et al*., 1997). Therefore, we compared *in vivo* levels of rhodopsin expression from various AAV expression constructs in mouse retinas. Eight AAV2/5 vectors incorporating different promoters and various elements were tested subsequent to subretinal delivery in wild type mice. Following AAV transduction in wild type mouse retinas, *RHO* mRNA expression of approximately 40% of that observed endogenously was achieved and RHO was detected in photoreceptor cells by immunocytochemistry. Notably, AAV transduction of *Rho*-/- mouse retinas with the most efficient expression vector not only resulted in RHO expression but the formation of ROS and a significant rod-derived ERG in treated eyes. In summary, a significant rescue of the severe retinopathy present in *Rho*-/- mice (Humphries *et al*., 1997; Lem *et al*., 1999) was observed.

Materials and Methods

Recombinant Adeno Associated Virus Preparation

Eight recombinant AAV2/5 (AAV) viruses were generated using a helper virus-free system as described (O'Reilly *et al*., 2007). Briefly, expression cassettes were cloned into pAAV-MCS (Stratagene), between the inverted terminal repeats of AAV2. The resulting constructs were transfected into human embryonic kidney (HEK)-293 cells (ATCC [accession number CRL-1573]) with pRep2/Cap521 and pHelper (Stratagene), at a ratio of 1:1:2. Fifty 150-mm plates of confluent cells were transfected using polyethylenimine. Forty-eight hours post-transfection, crude viral lysates were cleared and purified by $CsCl_2$-gradient centrifugation. AAV-containing fractions were dialyzed against PBS. Genomic titres (DNase-resistant viral particles per ml; vp/ml) were determined by qRT-PCR. AAV-*Rho*-P-*EGFP* and AAV-CMV-P-*EGFP* contained a 1.7kb mouse Rho promoter (*Rho*-P) or CMV-P-driven EGFP (Fig 1). A CMV-P sequence, β-globin intron and *HGH* poly-adenylation signal from pAAV-MCS (Accession No: AF396260.1; Stratagene, La Jolla, CA, USA) were used in AAV constructs (Fig 1). Constructs also contained a selection of other sequences such as *EGFP* coding sequence (Accession No: U55761), CMV enhancer (CMVE; Accession No: EF550208), minimal synthetic polyA (Levitt *et al*., 1989) and *WPRE* sequences (Accession No: J04514, Fig 1). A replacement human rhodopsin cDNA (*RHO*) sequence (*RHO*-BB) was constructed by modifying the wild type human *RHO* sequence (Accession No: NM_000539.2) at nt 254–274 as follows 5'-AT<u>A</u>AA<u>T</u>TT<u>TT</u>T<u>G</u>AC<u>C</u>CT<u>G</u>TA<u>T</u>-3' (altered bases underlined, O'Reilly *et al*., 2007) and was included in AAV-BB8, AAV-BB9, AAV-BB10, AAV-BB13, AAV-BB24 and

AAV-BB32. Conserved *Rho*-P elements are given in Supplemental Table 1. shBB (GTCAACTTCCTCACGCTCTATTCAAGAGATAGAGCGTGAGGA AGTTGATTTTT) targeting *RHO* mRNA at nt 254–274 was expressed from the H1 promoter (Accession No: X16612) and included in some constructs (H1PshBB, O'Reilly *et al*., 2007, Fig 1).

Subretinal AAV Injection, RNA Isolation and Analysis

Subretinal injections were performed in strict compliance with the European Communities Regulations 2002 and 2005 (Cruelty to Animals Act) and the Association for Research in Vision and Ophthalmology statement for the use of animals in ophthalmic and vision research as described (O'Reilly *et al*., 2007). Briefly, adult mice were anesthetized by intraperitoneal injection of medetomidine and ketamine (10 and 750 mg/10 g body weight, respectively). Pupils were dilated with 1% cyclopentolate and 2.5% phenylephrine, and, using topical anaesthesia (Amethocaine), a small puncture was made in the sclera. A 34-gauge blunt-ended microneedle attached to a 10 µl syringe (Hamilton) was inserted through the puncture, and AAV in PBS was administered to the subretinal space, and a retinal detachment was induced. Following subretinal injection, a reversing agent (100 mg/10 g body weight [Atipamezole Hydrochloride]) was delivered by intraperitoneal injection. Body temperature was maintained using a homeothermic heating device. Newborn (P0) mice were prepared for subretinal injection with the method described by Matsuda and Cepko (Matsuda and Cepko, 2004). Typically, two µl of 5 x 10^{12} vp/ml (1 x 10^{10} vp) AAV-*RHO* in PBS were administered to adult wild type 129 mice while 0.5 µl of 5 x 10^{12} vp/ml (2.5 x 10^{9} vp) or 1.3 x 10^{13} vp/ml (6.5 x 10^{9} vp)

were administered to P0 Rho-/- mice. Two µl of 1 x 10^{12} vp/ml (2 x 10^{9} vp) of AAV-*Rho*-P-*EGFP* and AAV-CMV-P-*EGFP* were injected into adult wild type 129 mice. RNA was isolated ten days or two weeks post injection and analysed by RNase protection or qRT-PCR as described (O'Reilly *et al*., 2007).

Morphologic Analyses by Light and Transmission Electron Microscopy (TEM)

Rhodopsin immunocytochemistry and fluorescent microscopy were performed as described (Kiang *et al*., 2005) two, six or twelve weeks post-injection. For RHO-specific immunocytochemistry, 3A6 primary rhodopsin antibody was used in 1:10 dilution. For tissue preparation for TEM a method previously described (Wolfrum, 1992) was slightly modified. Briefly, six weeks post-injection, AAV transduced eyes were enucleated, fixed in 4% paraformaldehyde in PBS, and whole mounted. Using the EGFP tracer, EGFP-positive and negative areas from the central part of the retinas were excised and fixed in 2.5% glutaraldehyde in 0.1 M Cacodylate buffer (pH 7.3) for 2 h at room temperature. Specimens were washed and fixed in buffered 2% OsO_4, dehydrated and embedded in araldite. Semi-thin (0.5 µm) and ultra-thin (60 nm) sections were cut on a Leica Ultracut S microtome. For light microscopy semi-thin sections were analysed with a Leica DM 6000 B microscope. Ultrastructural analyses were performed using a Tecnai 12 BioTwin transmission electron microscope (FEI, Eindhoven, NL) and imaged with a SIS MegaView III SCCD camera. ROS measurements were performed with analySIS software.

Electroretinography (ERG)

Rod isolated ERG recordings were prepared as described (Chadderton *et al*., 2009). Briefly, animals were dark-adapted overnight and all procedures carried out under dim red light. For anesthesia, Ketamine and Xylazine (16 and 1.6 mg/10g body weight, respectively) were injected intraperitoneally. Pupils were dilated with 1% Cyclopentalate and 2.5% Phenylephrine. Eyes were maintained in a proptosed position throughout the examination. Reference and ground electrodes were positioned subcutaneously, approximately 1 mm from the temporal canthus and anterior to the tail respectively. The ERG responses were recorded simultaneously from both eyes by means of goldwire electrodes (Roland Consult Gmbh), which were positioned to touch the central cornea of each eye. Corneal hydration and electrical contact were maintained throughout the examination by the application of a small drop of Vidisic (Dr. Mann Pharma, Berlin, Germany) to the cornea. Standardized flashes of light were presented to the mouse in a Ganzfeld bowl. Responses were analyzed using a RetiScan RetiPort electrophysiology unit (Roland Consulting Gmbh). The protocol used was based on that approved by the International Clinical Standards Committee for human ERG. Rod-isolated responses were recorded using a dim white flash (-25 dB maximal intensity where maximal flash intensity was 3 candelas/m^2/s) presented in the dark-adapted state. Following the standard convention, a-waves were measured from the baseline to the trough and b-waves from the baseline. Following ten minutes light adaptation (30 candelas/m^2) cone responses were recorded to the standard flash presented at 0.5 Hz and 10 Hz flicker against the rod supressing background.

Statistical Analysis

Means and standard deviation values (SD) of data sets were calculated. Statistical significance of differences between groups were determined by ANOVA using LSD post-hoc test (Data Desk 6.1, Data Descriptions Inc., New York, USA); differences of $p<0.05$ were considered statistically significant.

Results

The primary focus of the current study was optimisation of RHO expression from AAV vectors and *in vivo* evaluation of these vectors in *Rho*-/- mice. A comparative evaluation of a series of *RHO* constructs was undertaken in an attempt to optimise AAV-delivered *RHO* replacement expression in mouse retinas (Fig 1).

The CMV promoter (CMV-P) incorporated into AAV vectors has previously been shown to drive high levels of transgene expression in a wide variety of cell types (Ledherz *et al*., 2008; Li *et al*., 2008; Mueller and Flotte, 2008; Surace *et al*., 2008; Stieger *et al*., 2009). CMV-P and 1.7kb *Rho*-P driven *EGFP* expression vectors containing the human β-globin intron and the human growth hormone polyadenylation signal were constructed (AAV-CMV-P-*EGFP* and AAV-*Rho*-P-*EGFP*, Fig. 1). Subsequent to subretinal injection of adult wild type mice with 2 x 10^9 viral particles (vp)/eye of AAV-CMV-P-*EGFP* and AAV-*Rho*-P-*EGFP*, EGFP expression was analysed by histology, fluorescent activated cell sorting (FACS) and quantitative real-time reverse transcription polymerase chain reaction (qRT-PCR) two weeks post-injection. Histological analysis revealed strong EGFP expression in photoreceptor cell bodies and segments for both promoters (Fig. 2A and 2C); no expression was observed in other components of the retina. Retinas were then dissociated and analysed by FACS (Fig. 2B and 2D) to compare intensities of EGFP expression. Higher intensities of EGFP fluorescence were found in cells from retinas transduced with AAV-*Rho*-P-*EGFP* versus AAV-CMV-P-*EGFP* (Fig. 2B and 2D). Subsequently, the sorted cells were used for qRT-PCR analysis (Fig. 2E), which revealed

approximately a 5-fold ($p<0.001$, $n=3$) higher mRNA level in cells from retinas transduced with AAV-*Rho*-P-*EGFP*. The higher level of expression achieved with *Rho*-P comparative to CMV-P, stimulated additional engineering of the retina-specific *Rho*-P to augment expression levels, rather than further exploration of a general promoter such as CMV-P.

Following the initial promoter experiments involving AAV-mediated EGFP expression in murine retina, six *RHO* replacement constructs termed AAV-BB8 (O'Reilly *et al*., 2007), AAV-BB9, AAV-BB10, AAV-BB13, AAV-BB24 and AAV-BB32 were engineered (Fig 1). Construct designs were constrained by the insert size limitation for AAV vectors (approximately 4.5kb). One set of constructs included large segments of the murine *Rho*-P while the other set of constructs included a shorter *Rho-P* complemented with CMV enhancer and/or WPRE sequences (Fig. 1). More specifically, AAV-BB8, AAV-BB9, AAV-BB24 and AAV-BB32 included a 1.7kb *Rho*-P whereas AAV-BB10 and AAV-BB13 contained a 0.5kb *Rho*-P augmented with the CMV enhancer element. AAV-BB13 contained a modified *WPRE* element (Loeb *et al*., 1999). In addition, a 0.7kb fragment of the endogenous *RHO* 3'-UTR (including poly-adenylation signals) was present in all vectors except AAV-BB24 and AAV-BB32. Multiple sequence alignments enabled comparison of rhodopsin promoter sequences from various species thereby highlighting conserved regions (Supplemental Table 1). AAV-BB24 and AAV-BB32 contained the 1.7kb *Rho*-P together with conserved elements of a 1.9kb fragment of *Rho*-P (Supplemental Table 1; Fig 1), a 0.4kb fragment of the endogenous 3'-UTR and a minimal poly-adenylation signal (Levitt *et al*., 1989). AAV-BB8, AAV-BB10, AAV-

BB13 and AAV-BB32 were generated with the H1 promoter driven shRNA suppressor cassette (H1PshBB), while AAV-BB9 and AAV-BB24 were generated without this cassette. Subsequently, AAV viral preparations in the range of 10^{12}-10^{13} vp/ml were produced from AAV-BB constructs.

In vivo RHO mRNA expression levels in RNA samples extracted from whole retinas achieved from the six AAV vectors described above were compared in adult wild type mice subsequent to subretinal administration of 1 x 10^{10} vp/eye of each virus (n=10). Levels of *RHO* expression in whole retina achieved from AAV vectors were compared to levels of *RHO* expression observed in *RHO*-M+/-*Rho*-/- mice, which express a *RHO* replacement gene (at 70% of endogenous *Rho* levels in wild type mice; O'Reilly *et al*., 2007; 2008) and display a normal retinal phenotype as evaluated by histology and ERG (O'Reilly *et al*., 2008). Ten days post-injection of AAV vectors, whole retinas were harvested and RNA isolated. *RHO* mRNA expression in wild type mice treated with AAV constructs, and *RHO*-M+/-*Rho*-/- mice, was confirmed by RNase protection assay (data not shown) and expression levels determined by qRT-PCR (Fig 3). Significant *RHO* mRNA expression from AAV-BB8, AAV-BB9 and AAV-BB10 was detected. However given the high levels of RHO found endogenously this expression represented up to 2% of that found in *RHO*-M+/-*Rho*-/- mice ($p<0.001$, Fig 3). No *RHO* mRNA amplification was observed in uninjected wild type mice (data not shown). In contrast to AAV-BB8, AAV-BB9 and AAV-BB10, *RHO* mRNA expression levels from AAV-BB13, AAV-BB24 and AAV-BB32 were significantly higher, i.e. 39-66% of that found in *RHO*-M+/-*Rho*-/- mice ($p<0.001$), representing approximately 40% of that found in wild type mice.

RHO expression increased by 30-fold ($p<0.001$), 50-fold ($p<0.001$) and 51-fold ($p<0.001$) in eyes injected with AAV-BB13, AAV-BB24 and AAV-BB32 respectively when compared to pAAV-BB8 (Fig 3). While the objective of the study was to achieve potent expression of RHO from AAV vectors, comparison of expression between identical vectors except for the addition of the shRNA suppressor, that is, AAV-BB8 versus AAV-BB9 or AAV-BB24 versus AAV-BB32 (Fig 1), suggested that the H1PshBB suppressor present in AAV-BB8 and AAV-BB32 did not significantly influence expression of the replacement *RHO* gene (Fig 3).

To analyse AAV-mediated RHO expression at the protein level, subretinal injections of AAV-BB8, AAV-BB13, AAV-BB24 (1×10^{10} vp/eye) and AAV-CMV-P-*EGFP* vectors (2×10^{9} vp/eye) were undertaken in adult wild type mice. The *RHO*-BB AAVs were co-injected with $1/10^{th}$ of AAV-CMV-P-*EGFP* tracer to facilitate localisation of transduced areas of retinas. Two weeks post-injection, immunocytochemistry using rhodopsin antibody which detects the human protein but not that of the mouse, was undertaken (Fig. 4). Significantly higher levels of RHO expression in retinas administered with AAV-BB13 (Fig 4E and 4F) or AAV-BB24 (Fig 4G and 4H) were obtained when compared to AAV-BB8 (Figure 4C and 4D). RHO labelling was confined to the photoreceptor segment layer (PSL) while EGFP was expressed in both the outer nuclear layer (ONL) and the PSL. *RHO*-M *Rho*-/- transgenic mice and AAV-CMV-P-*EGFP* subretinal administration were used as controls for RHO labelling (Fig. 4I and 4J) and injections (Fig. 4A and 4B) respectively.

Two constructs, AAV-BB13 and AAV-BB24, expressing high levels of rhodopsin mRNA and protein in wild type mice were further explored as a means to express *RHO* in *Rho*-/- mice. Initially, subretinal delivery of 3.9 x 10^9 vp/eye of AAV-BB13 and AAV-BB24 vectors (including $1/10^{th}$ of AAV-CMV-P-*EGFP* tracer) was undertaken in *Rho*-/- mice at P0 (n=5) and expression analysed by immunocytochemistry six weeks post-injection. Significant RHO expression in the ONL and PSL, co-localised with the EGFP tracer, was detected in treated *Rho*-/- mouse retinas using both AAV vectors (Fig. 5C-F). The pattern of RHO labelling observed resembled that found in wild type mouse retinas and the morphology of PSL suggested the presence of ROS in treated *Rho*-/- mouse eyes (Fig. 5E and 5F). In contrast, RHO immunolabelling (or EGFP expression) was not observed in un-injected eyes (Fig. 5A and 5B). As is well documented, ROS do not develop in *Rho*-/- retinas (Humphries *et al*., 1997). Analysis of AAV-BB24 (3.9 x 10^9 vp/eye) transduced *Rho*-/- mouse retinas at twelve weeks post injection (n=5, Fig. 6) indicated a similar pattern of RHO expression (Fig. 6C and 6D) to that observed at six weeks (Fig. 5). Photoreceptor cell numbers were decreased relative to the six week timepoint (Fig. 5) but still consisted of three to four rows of ONL (Fig. 6C and 6D), while in un-injected control eyes the ONL was comprised of just a single cell row of cone nuclei (Fig. 6B).

A more extensive analysis was undertaken using AAV-BB24. Two different doses of 3.9 x 10^9 vp/eye (n=10) and 6.5 x 10^9 vp/eye of AAV-BB24 (n=3) both including $1/10^{th}$ of pAAV-CMV-P-*EGFP* tracer were subretinally injected into right eyes of *Rho*-/- mice at P0 while the left eyes were un-injected; AAV-*Rho*P-*EGFP* and PBS were used as

controls for injection. Six weeks post-injection, ERG analyses were undertaken on the injected and control eyes from these mice. Notably, rod-isolated ERG recordings of AAV-BB24 injected *Rho*-/- mouse eyes provided evidence of significant rod photoreceptor function compared to fellow un-injected *Rho*-/- eyes in which rod-generated responses were not detected (Figure 7). In the un-injected versus injected eyes, means of rod-isolated b-wave amplitudes were 4.0±5.2 μV compared to 37.6±14.5 μV ($p<0.001$; Fig. 7A and B) at the lower AAV dose while 4.7±3.6 μV compared to 135.3±58.5 μV ($p<0.05$; Fig 7C and D) at the higher AAV dose. The mean value of control rod isolated b-wave amplitudes was 703.6±116.1 μV (n=8) in age-matched *RHO*-M mice (Fig 7E and F). In contrast, cone-isolated ERGs (b-wave amplitudes; Suppl. Fig. 1) were found to be compromised in AAV-BB24 injected eyes (29.0±13.7 μV, n=10, $p<0.01$) when compared to un-injected eyes (89.4±28.9 μV, n=14). Notably, control AAV-*Rho*P-*EGFP* (not shown) and PBS injected eyes (33.18±19.3 μV, n=4, $p<0.01$) showed similarly decreased cone-isolated b-wave amplitudes, which were not significantly different from AAV-BB24 injected eyes ($p=0.54$). Cone function was less impaired when injections were undertaken at P10, however, most injections were undertaken at P0 to ensure early delivery of RHO.

In a further set of experiments, rod-isolated ERGs were compared at six and twelve weeks following injection of AAV-BB24 at P0 (3.9×10^{12} vp/eye, n=12) into right eyes while left eyes were un-injected. Considerable rod-ERG was detected at twelve weeks post-injection (20.6±19.3 μV, Fig. 8) but b-wave amplitudes were significantly lower than at six weeks (61.9±35.6 μV, $p<0.01$, Fig. 8). Although the b-wave amplitudes

varied, a general trend of decrease in b-wave amplitudes of individual animals was observed between six and twelve weeks (Fig. 8). Notably, no rod function was detected in control un-injected eyes at either six (Fig. 7) or twelve weeks (not shown).

Histology of the AAV-BB24 tranduced *Rho*-/- retinas was further analysed at the ultrastructural level six weeks post-injection with 6.5 x 10^9 vp of AAV-BB24 (n=3) including 1/10^{th} of AAV-CMV-P-*EGFP* tracer. Paraformaldehyde fixed eyes were whole mounted and using the EGFP tracer transduced and un-transduced areas identified; the transduced area covered by a single injection was 38.8±7.9% of the retina (n=3, Fig 9B). Representative areas of un-injected (Fig 9A), injected un-transduced and injected transduced (Fig 9B) retinas were excised and processed for resin embedding. Semithin sections from these eyes (Fig 9C, E and G) indicate a marked protection of retinal structure in the AAV-BB24 transduced areas (Fig 9G) including more extensive nuclear and photoreceptor segment layers compared to the un-transduced or un-injected areas (Fig 9C and E). Using transmission electron microscopy (TEM) ROS were detected in the AAV-BB24 transduced areas, with ROS reaching up to the retinal pigment epithelium (RPE) (Fig 9H). Only rod photoreceptor inner segments (RIS) were detected in the un-transduced or un-injected retinal areas (Fig 9D and F); also note the wide extracellular space between the photoreceptor segments and the RPE cells which was confirmed at higher magnification (Fig 10A). TEM at higher magnification also revealed that RIS in the un-transduced areas possessed ciliary processes (connecting cilium), which in wild type photoreceptors connect the inner and the outer segments. However, in these photoreceptors, truncated outer segments lacking membrane discs were observed at the

outer tips of the connecting cilia (Fig 10A). On the contrary, in the transduced areas correctly formed ROS with parallel membrane discs typical of rod photoreceptor cells attached to the connecting cilium were present. The lengths of the ROS were found to be 9.52±1.08 μm (n=9). Note that the average length of the ROS in wild type mouse retinas is 23.8±1.32 μm (Nickell *et al*., 2007). The ROS of the rescued photoreceptors connected to the RPE (Fig 10C) and disc membrane stacks shed from the ROS tips appeared to be phagocytosed by the cells of RPE (Supplemental Fig 2). Correctly formed discs in the ROS of rescued photoreceptors resembled corresponding structures in wild type retinas (Fig 10D).

Discussion

GPCRs constitute an enormous family of transmembrane molecules involved in signal transduction and are fundamental to a multiplicity of cellular processes (Palczewski, 2006). Rhodopsin represents one of the most extensively studied GPCRs; investigations facilitated by the relatively large quantities of protein found in the disc membranes of rod photoreceptor cells. The continual replenishing of ROS, in which rhodopsin represents 90% of the protein content, suggests that extensive renewal with *de novo* rhodopsin molecules is required for optimal visual function (Palczewski, 2006, Winkler, 2008). The high level of rhodopsin expression in ROS, while advantageous for early studies focused on delineating the function of the protein in phototransduction, presents a significant challenge in terms of gene therapy where the principal objective is to recapitulate endogenous levels of rhodopsin expression from an exogenously delivered vector. Therefore the focus of the current study was to explore ways to achieve replacement RHO expression from AAV at appropriate levels for *in vivo* biological functionality.

When selecting a viral vector for gene delivery various issues must be considered including tropism of the vector for the target cell, the viral titres that can be achieved, the safety and immune tolerance associated with the virus and available clinical information regarding administration to humans. Given these issues, AAV represents an attractive vector option for photoreceptors (Ledherz *et al*., 2008; Li *et al*., 2008; Surace *et al*., 2008; Stieger *et al*., 2009). However AAV has limited capacity of approximately 4.5kb for most serotypes thereby curtailing the insert size that can be engineered into AAV. Larger

inserts of approximately 9kb have been incorporated into AAV2/5 (Allocca *et al*., 2008), although levels of expression from these vectors have still to be fully elucidated. In the current study, to explore the feasibility of achieving high levels of expression of a *RHO* replacement gene, a range of AAV *RHO* replacement vectors were produced. A human *RHO* replacement gene was used which was modified such that it is resistant to the shRNA expressed from H1PshBB but encodes wild type RHO. The replacement gene characterised in this study may be of value in future human suppression and replacement therapies.

Expression levels provided by CMV-P and the 1.7kb *Rho*-P were determined using AAV-CMV-P-*EGFP* and AAV-*Rho*-P-*EGFP* respectively (Fig 2). *Rho*-P was found to result in 5-fold higher levels of RHO expression than CMV-P in murine retinas (Fig 2) and therefore for reasons of specificity and superior expression, this promoter was progressed further. A subsequent comparative analysis of six AAV *Rho*-P *RHO* replacement constructs was undertaken *in vivo* to assess levels of RHO expression achieved utilising these vectors. Expression levels of *RHO* mRNA were determined in RNA samples extracted from whole retinas. Therefore the *RHO* mRNA expression levels in the transduced areas were expected to be higher.

Notably, *RHO* promoter driven expression of EGFP and RHO resulted in a differential subcellular distribution of the two proteins in the adult retina. EGFP was localized in the cell body (Fig 2) and RIS while RHO was mainly detected in ROS (Fig 4). Recent evidence suggests that trafficking to ROS represents the default location for photoreceptor membrane proteins such as RHO (Baker *et al*., 2008) and that membrane

proteins locate elsewhere only if they contain specific targeting signals (Baker *et al*., 2008). Additionally, a ROS-targeting signal in the C-terminus of RHO has been reported (Tai *et al*., 1999; Deretic, 2006). On the other hand, EGFP, a soluble protein localizes in the cytosol including the cell body and RIS but is not evident in ROS. Sequential inclusion/exclusion of various elements and conserved sequences associated with the rhodopsin promoters in AAV vectors served to improve significantly expression of the *RHO* replacement gene (Figs 1 and 3; Supplemental Table 1). In particular, inclusion of the WPRE sequence or regions of the murine *Rho*-P served to radically increase rhodopsin expression. RNA results were mirrored by evaluation of RHO protein expression in wild type (Fig 4) and *Rho*-/- mice (Fig 5 and 6). WPRE was included in AAV-BB13 3' of the first poly-adenylation signal to minimize read through and aid poly-adenylation (Higashimoto *et al*., 2007). Note that RHO is mainly localized to the ROS in adult retinas (Fig 4), while it is also detected in the cell bodies of rods in the developing retina (Fig 5 and 6). The mechanisms underlying such improvements in expression may possibly be related to the presence of binding sites for transcription factors such as Neural Retinal Leucine zipper factor (NRL) and Cone Rod homeobox-containing transcription factor (CRX) in the *Rho*-P sequences used (Hennig et al., 2008; Oh et al., 2008).

As the inclusion of additional murine *Rho*-P sequences in AAV-BB24 provided high levels of RHO expression, a detailed analysis was undertaken with this vector in *Rho*-/- mice. Subretinal delivery of AAV-BB24 to P0 *Rho*-/- mice followed by ERG at six and twelve weeks post administration of virus provided evidence of significant rod photoreceptor-derived ERG responses in *Rho*-/- mice (Fig 7 and 8). The rod-derived

amplitudes declined with time and this was mirrored by reduced ONL thickness (Fig 6), at twelve weeks post-injection. However, there was a clearly visible improvement compared to un-injected eyes where only a single photoreceptor cell layer remained and no recordable rod-ERG response was detected. Compromised cone-ERG was observed in *Rho*-/- mice injected with AAV-BB24 or PBS alone at P0 (Supplemental Fig 1); causative mechanisms will require future investigation in terms of possible surgical trauma. Notably, less of a decrease in b-wave amplitude was observed in mice subretinally injected at P10. Transmission electron microscopy (TEM) provided unequivocal evidence of the presence of ROS in AAV-BB24-treated *Rho*-/- mouse eyes (Fig 9, Fig 10 and Supplemental Fig 2). Indeed the lengths of the AAV-BB24-induced ROS were in the order of one third those present in wild type mice (Nickell *et al*., 2007). While the capability of retinal structures such as ROS for plasticity and recovery has still to be fully elucidated, the current study provides some additional insights into this feature of ROS (Schremser and Williams, 1995; Liang *et al*., 2004; Wen *et al*., 2009).

The aim of the study was to develop AAV-*RHO* vectors that can achieve levels of *RHO* gene expression, which provide functional rods in *Rho*-/- mice. While this in itself was a significant achievement, it was also demonstrated that the presence of an RNAi-based suppressor gene (H1PshBB; targeting wild type *RHO*) in some vectors did not influence expression of the sequence-modified *RHO*-BB replacement gene (Figure 1 and 3), mirroring the results from a prior study *in vitro* (O'Reilly *et al*. 2007). Such RNAi suppressors and RNAi-resistant replacement genes will be required as components of future therapies, in particular for gain-of-function *RHO* mutations, where potent

suppression in conjunction with efficient rhodopsin replacement may provide therapeutic benefit for *RHO*-adRP.

It is worth highlighting challenges associated with ameliorating the *Rho*-/- phenotype by gene replacement. Rho expression initiates at approximately P4 post-natally in the murine retina (McNally *et al*., 1999) increasing in levels of expression until Rho comprises 90% of ROS disc membranes (Palczewski, 2006). To increase the likelihood that the appropriate cellular machinery accompanying Rho expression from P4 is invoked at the correct timeframe in AAV-BB24 treated *Rho*-/- mice, it was deemed optimal to deliver AAV-BB24 early, that is, at P0. Even using P0 injections, initial histologically observable expression from the AAV2/5 serotype occurs approximately one week post-injection in murine retinas. The volume, and hence viral dose, that can be injected subretinally into P0 mice is limited to 0.5 μls. Moreover, viral spread in P0 *Rho*-/- mice is limited (Fig 9B), thereby also restricting the extent of possible rescue. Since AAV has a modest insert capacity, recapitulating endogenous levels of rhodopsin from AAV vectors is a significant task. However, in the current study we have made considerable strides towards achieving this goal with associated significant structural and functional benefits in *Rho*-/- mice.

Despite the limitations and challenges outlined above, this is the first demonstration of substantial rescue of aspects of the retinal degeneration in *Rho*-/- mice that lack this highly expressed GPCR. The study also represents significant progress towards the

development of gene-based therapies for RHO-adRP, the most common form of RP by providing a functionally relevant replacement rhodopsin gene.

Acknowledgments

We thank Prof. W. Baehr, (University of Utah, Salt Lake City, UT) for the original RHO cDNA construct, Prof. German and Prof. Hope for the woodchucks (The Salk Institute, La Jolla, CA), Prof. R.S. Molday (University of British Colombia, Vancouver BC, CA) for the two rhodopsin primary antibodies, Dr. Alfonso Blanco Fernandez (Flow Cytometry Core Facility, University College, Dublin) for assisting with FACS analysis, Elisabeth Sehn (University of Mainz) for skilful technical assistance and the staff of the Bioresources Unit, Trinity College Dublin. This work was supported by Science Foundation Ireland; Fighting Blindness Ireland, Enterprise Ireland; European Union RETNET [MRT-CT-2003-504003]; EviGenoRet [LSHG-CT-2005-512036]; Deutsche Forschungsgemeinschaft (GRK1044/1); and FAUN-Stiftung.

Author Disclosure Statement

J.F. and P.K. are directors in Genable Technologies, S.M-W., N.C., A.P. and M.O'R. are consultants for Genable Technologies. The above authors have competing interests.

References

Acland, G.M., Aguirre, G.D., Ray, J., Zhang, Q., Aleman, T.S., Cideciyan, A.V., Pearce-Kelling, S.E., Anand, V., Zeng, Y., Maguire, A.M., Jacobson, S.G., Hauswirth, W.W., and Bennett, J. (2001). Gene therapy restores vision in a canine model of childhood blindness. Nat Gen. 28, 92-95.

Allocca, M., Doria, M., Petrillo, M., Colella. P., Garcia-Hoyo, M., Gibbs, D., Kim, S.R., Maguire, A., Rex, T.S., Di Vicino, U, Cutillo, L., Sparrow, J.R., Williams, D.S., Bennett, J., Auricchio, A. (2008). Serotype-dependent packaging of large genes in adeno-associated viral vectors results in effective gene delivery in mice. J. Clin. Invest. 118, 1955-1964.

Bainbridge, J.W., Smith, A.J., Barker, S.S., Robbie, S., Henderson, R., Balaggan, K., Viswanathan, A., Holder, G.E., Stockman, A., Tyler, N., Petersen-Jones, S., Bhattacharya, S.S., Thrasher, A.J., Fitzke, F.W., Carter, B.J., Rubin, G.S., Moore, A.T., and Ali, R.R. (2008). Effect of gene therapy on visual function in Leber's congenital amaurosis. N. Engl. J. Med. 358, 2231-2239.

Baker, S.A., Haeri, M., Yoo, P., Gospe, S.M. 3rd, Skiba, N.P., Knox, B.E. and Arshavsky, V.Y. (2008). The outer segment serves as a default destination for the trafficking of membrane proteins in photoreceptors. J Cell Biol. 183, 485-498.

Bhatti, M.T. (2006). Retinitis pigmentosa, pigmentary retinopathies, and neurologic diseases. Curr Neurol Neurosci Rep. 6, 403-413.

Cashman, S.M., Binkley, E.A., and Kumar-Singh, R. (2005). Towards mutation-independent silencing of genes involved in retinal degeneration by RNA interference. Gene Ther. 12, 1223-1228.

Chadderton, N., Millington-Ward, S., Palfi, A., O'Reilly, M., Tuohy, G., Humphries, M.M., Li, T., Humphries, P., Kenna, P.F., and Farrar, G.J. (2009). Improved retinal function in a mouse model of dominant retinitis pigmentosa following AAV-delivered gene therapy. Mol Ther. 17, 593-9.

Cideciyan, A.V., Aleman, T.S., Boye, S.L., Schwartz, S.B., Kaushal, S., Roman, A.J., Pang, J.J., Sumaroka, A., Windsor, E.A., Wilson, J.M., Flotte, T.R., Fishman, G.A., Heon, E., Stone, E.M., Byrne, B.J., Jacobson, S.G., and Hauswirth, W.W. (2008). Human gene therapy for RPE65 isomerase deficiency activates the retinoid cycle of vision but with slow rod kinetics. Proc. Natl. Acad. Sci. USA. 105, 15112-15117.

Deretic, D. (2006). A role for rhodopsin in a signal transduction cascade that regulates membrane trafficking and photoreceptor polarity. Vision Res. 46, 4427-4433.

Dryja, T.P., McGee, T.L., Reichel, E., Hahn, L.B., Cowley, G.S., Yandell, D.W., Sandberg, M.A., and Berson, E.L. (1990). A point mutation of the rhodopsin gene in one form of retinitis pigmentosa. Nature. 343, 364-266.

Farrar, G.J., Kenna, P.F., and Humphries, P. (2002). On the genetics of retinitis pigmentosa and on mutation-independent approaches to therapeutic intervention. EMBO J. 21, 857-864.

Farrar, G.J., McWilliam, P., Bradley, D.G., Kenna, P., Lawler, M., Sharp, E.M., Humphries, M.M., Eiberg, H., Conneally, P.M., Trofatter, J.A., and Humphries, P. (1990). Autosomal dominant retinitis pigmentosa: linkage to rhodopsin and evidence for genetic heterogeneity. Genomics. 8, 35-40.

Gorbatyuk, M., Justilien, V., Liu, J., Hauswirth, W.W., and Lewin, A.S. (2007). Preservation of photoreceptor morphology and function in P23H rats using an allele independent ribozyme. Exp. Eye Res. 84, 44-52.

Hamm, H.E., Deretic, D., Arendt, A., Hargrave, P.A., Koenig, B., and Hofmann, K.P. (1988). Site of G protein binding to rhodopsin mapped with synthetic peptides from the alpha subunit. Science. 241, 832-835.

Hennig, A.K., Peng G-H. and Chen, S. (2008). Regulation of photoreceptor gene expression by CRX-associated transcription factor network. Brain Res. 1192, 114-133.

Higashimoto, T., Urbinati, F., Perumbeti, A., Jiang, G., Zarzuela, A., Chang, L.J., Kohn, D.B. and Malik, P. (2007). The woodchuck hepatitis virus post-transcriptional regulatory element reduces readthrough transcription from retroviral vectors. Gene Ther. 14, 1298-1304.

Hobson, A.H., Donovan, M., Humphries MM, Tuohy G, McNally N, Carmody R, Cotter T, Farrar GJ, Kenna PF, Humphries P. (2000). Apoptotic photoreceptor death in the rhodopsin knockout mouse in the presence and absence of c-fos. Exp Eye Res. 71, 247-254.

Humphries, M.M., Rancourt, D., Farrar, G.J., Kenna, P., Hazel, M., Bush, R.A., Sieving, P.A., Sheils, D.M., McNally, N., Creighton, P., Erven, A., Boros, A., Gulya, K., Capecchi, M.R., and Humphries, P. (1997). Retinopathy induced in mice by targeted disruption of the rhodopsin gene. Nature Genetics. 15, 216-219.

Kiang, A.S., Palfi, A., Ader M, Kenna PF, Millington-Ward S, Clark G, Kennan A, O'Reilly M, Tam LC, Aherne A, McNally, N., Humphries, P., and Farrar G.J. (2005). Toward a gene therapy for dominant disease: validation of an RNA interference-based mutation-independent approach. Mol. Ther. 12, 555-561.

LaVail, M.M., Yasumura, D., Matthes MT, Drenser KA, Flannery JG, Lewin AS, and Hauswirth WW. (2000). Ribozyme rescue of photoreceptor cells in P23H transgenic rats: long-term survival and late-stage therapy. Proc. Natl. Acad. Sci. USA. 97, 11488-11493.

Le Meur, G., Stieger, K., Smith, A.J., Weber, M., Deschamps, J.Y., Nivard, D., Mendes-Madeira, A., Provost, N., Péréon, Y., Cherel, Y., Ali, R.R., Hamel, C., Moullier, P., and Rolling, F. (2007). Restoration of vision in RPE65-deficient Briard dogs using an AAV

serotype 4 vector that specifically targets the retinal pigmented epithelium. Gene Ther. 14, 292-303.

Lebherz, C., Maguire, A., Tang, W., Bennett, J., and Wilson, J.M. (2008). Novel AAV serotypes for improved ocular gene transfer. J Gene Med. 10, 375-382.

Lem, J., Krasnoperova, N.V., Calvert, P.D., Kosaras, B., Cameron, D.A., Nicolò, M., Makino, C.L., Sidman, R.L. (1999). Morphological, physiological, and biochemical changes in rhodopsin knockout mice. Proc Natl Acad Sci USA. 96, 736-741.

Levitt, N., Briggs, D., Gil, A. and Proudfoot, N.J. (1989). Definition of an efficient synthetic poly(A) site. Genes Dev. 3, 1019-1025.

Lewin, A.S., Drenser, K.A., Hauswirth W.W., Nishikawa, S., Yasumura, D., Flannery, J.G. and LaVail, M.M. (1998). Ribozyme rescue of photoreceptor cells in a transgenic rat model of autosomal dominant retinitis pigmentosa. Nat Med. 8, 967-971.

Li, Q., Miller, R., Han, P.Y., Pang, J., Dinculescu, A., Chiodo, V., Hauswirth, W.W. (2008). Intraocular route of AAV2 vector administration defines humoral immune response and therapeutic potential. Mol Vis. 14, 1760-1769.

Li, T., Snyder, W.K., Olsson, J.E, and Dryja, T.P. (1996). Transgenic mice carrying the dominant rhodopsin mutation P347S: Evidence for defective vectorial transport of rhodopsin to the outer segments. Proc. Natl. Acad. Sci. USA. 93, 14176–14181.

Liang, Y., Fotiadis, D., Maeda, T., Maeda, A., Modzelewska, A., Filipek, S., Saperstein, D.A., Engel, A. and Palczewski, K. (2004). Rhodopsin signaling and organization in heterozygote rhodopsin knockout mice. J Biol Chem. 279, 48189-48196.

Lodowski, D.T., Angel T.E., and Palczewski, K. (2009). Comparative analysis of GPCR crystal structures. Photochemistry and Photobiology. 85, 425-430.

Loeb, J.E., Cordier, W.S., Harris, M.E., Weirzman, M.D., and Hope, T.J. (1999). Enhanced Expression of Transgenes from Adeno-Associated Virus Vectors with the Woodchuck Hepatitis Virus Posttranscriptional Regulatory Element: Implications for Gene Therapy. Human Gene Ther. 10, 2295–2305.

Maguire, A.M., Simonelli, F., Pierce, E.A., Pugh, E.N. Jr, Mingozzi, F., Bennicelli, J., Banfi, S., Marshall, K.A., Testa, F., Surace, E.M., Rossi, S., Lyubarsky, A., Arruda, V.R., Konkle., B., Stone E, Sun, J., Jacobs, J., Dell'Osso, L., Hertle, R., Ma, J.X., Redmond, T.M., Zhu, X., Hauck, B., Zelenaia, O., Shindler, K.S., Maguire, M.G., Wright, J.F., Volpe, N.J., McDonnell, J.W., Auricchio, A., High, K.A., and Bennett, J. (2008). Safety and efficacy of gene transfer for Leber's congenital amaurosis. N. Engl. J. Med. 358, 2240-2248.

Matsuda, T. and Cepko, C.L. (2004). Electroporation and RNA interference in the rodent retina in vivo and in vitro. Proc Natl Acad Sci USA. 101, 16–22.

McNally, N., Kenna, P., Humphries, M.M., Hobson, A.H., Khan, N.N., Bush, R.A., Sieving, P.A., Humphries, P. and Farrar, G.J. (1999). Structural and functional rescue of murine rod photoreceptors by human rhodopsin transgene. Human Mol Genet. 8, 1309-1312.

McWilliam, P., Farrar, G.J., Kenna, P., Bradley, D.G., Humphries, M.M., Sharp, E.M., McConnell, D.J., Lawler, M., Sheils, D., Ryan, C., and Humphries, P. (1989). Autosomal dominant retinitis pigmentosa (ADRP): localization of an ADRP gene to the long arm of chromosome 3. Genomics. 5, 619-622.

Millington-Ward, S., O'Neill, B., Tuohy, G., Al-Jandal, N., Kiang, A.S., Kenna, P.F., Palfi, A., Hayden, P., Mansergh, F., Kennan, A., Humphries, P. and Farrar, G.J. (1997). Strategems in vitro for gene therapies directed to dominant mutations. Hum. Mol. Genet. 6, 1415-1426.

Mueller, C., and Flotte, T.R. (2008). Clinical gene therapy using recombinant adeno-associated virus vectors. Gene Ther. 15, 858-63. Review.

Nickell, S., Park, P. S-H., Baumeister, W., and Palczewski K. (2007). Three dimensional architecture of murine rod outer segments determined by cryoelectron tomography. J Cell Biol. 177, 917-925.

O'Reilly, M., Millington-Ward, S., Palfi, A., Chadderton, N., Cronin, T.C., McNally, N., Humphries, M.M., Humphries, P., Kenna, P.F. and Farrar, G.J. (2008). A transgenic

mouse model for gene therapy of rhodopsin-linked Retinitis Pigmentosa. Vision Research. 48, 386-391.

O'Reilly, M., Palfi, A., Chadderton N, Millington-Ward S, Ader M, Cronin T, Tuohy T, Auricchio A, Hildinger M, Tivnan, McNally, N., Humphries, M.M., Kiang, A.S., Humphries, P., Kenna, P.F., and Farrar, G.J. (2007). RNA interference-mediated suppression and replacement of human rhodopsin in vivo. Am. J. Hum. Genet. 81, 127-135.

Oh, E.C., Cheng, H, Hao, H., Jia, L., Khan N.W. and Swaroop, A. (2008). Rod differentiation factor NRL actovates the expression of nuclear receptor NR2E3 to suppress the development of cone photoreceptors. Brain Res. 1236, 16-29.

Olsson, J.E., Gordon, J.W., Pawlyk, B.S., Roof, D., Hayes, A., Molday, R.S., Mukai, S., Cowley, G.S., Berson, E.L., and Dryja, T.P. (1992). Transgenic mice with a rhodopsin mutation (Pro23His): a mouse model of autosomal dominant retinitis pigmentosa. Neuron. 9, 815-830.

Palczewski, K. (2006). G protein-coupled receptor rhodopsin. Annu Rev Biochem. 75, 743-767.

Palfi, A., Ader, M., Kiang AS, Millington-Ward S, Clark G, O'Reilly M, McMahon HP, Kenna PF, Humphries P, and Farrar GJ. (2006). RNAi-based suppression and replacement of rds-peripherin in retinal organotypic culture. Hum. Mutat. 27, 260-268.

Schremser, J.L and Williams, T.P. (1995). Rod outer segment (ROS) renewal as a mechanism for adaptation to a new intensity environment. I. Rhodopsin levels and ROS length. Exp Eye Res. 61, 17-23.

Stieger, K., Schroeder, J., Provost, N., Mendes-Madeira, A., Belbellaa, B., Le Meur, G., Weber, M., Deschamps, J.Y., Lorenz, B., Moullier, P., and Rolling, F. (2009). Detection of intact rAAV particles up to 6 years after successful gene transfer in the retina of dogs and primates. Mol Ther. 17, 516-523.

Surace, E.M., and Auricchio, A. (2008). Versatility of AAV vectors for retinal gene transfer. Vision Res. 48, 353-359.

Tai, A.W., Chuang, J.Z., Bode, C., Wolfrum, U. and Sung, C.H. (1999). Rhodopsin's carboxy-terminal cytoplasmic tail acts as a membrane receptor for cytoplasmic dynein by binding to the dynein light chain Tctex-1. Cell. 97, 877-887.

Tan, M.H., Smith, A.J., Pawlyk, B., Xu, X., Liu, X., Bainbridge, J.B., Basche, M., McIntosh, J,. Tran., H.V., Nathwani, Li, T., and Ali, R.R.. (2009). Gene therapy for retinitis pigmentosa and Leber congenital amaurosis caused by defects in AIPL1: effective rescue of mouse models of partial and complete Aipl1 deficiency using AAV2/2 and AAV2/8 vectors. Hum Mol Genet. 18, 2099-114.

Unger, V.M., Hargrave, P.A., Baldwin, J.M., and Schertler, G.F. (1997). Arrangement of rhodopsin transmembrane alpha-helices. Nature. 389, 203-206.

Wen, X.H., Shen, L., Brush, R.S., Michaud, N., Al-Ubaidi, M.R., Gurevich, V.V., Hamm, H.E., Lem, J., Dibenedetto, E., Anderson, R.E. and Makino, C.L. (2009). Overexpression of rhodopsin alters the structure and photoresponse of rod photoreceptors. Biophys J. 96, 939-950.

Winkler, B.S. (2008). An hypothesis to account for the renewal of outer segments in rod and cone photoreceptor cells: renewal as a surrogate antioxidant. Invest Ophthalmol Vis Sci. 49, 3259-3261.

Wolfrum, U. (1992). Cytoskeletal elements in athropod sensilla and mammalian photoreceptors. Biol Cell. 76, 373-381.

Legends

Figure 1. Schematic representation of AAV vector constructs

EGFP was expressed using either the CMV immediate early promoter (CMV-P) or the 1.7kb fragment of the rhodopsin promoter (1.7 *Rho*-P). Replacement rhodopsin-BB (*RHO*-BB) was expressed using a 1.7kb or a 0.5kb fragments of the *Rho*-P, while shBB RNA was expressed from the H1 promoter (H1shBB). The *RHO*-BB replacement and the H1shBB expression cassettes were separated by a spacer fragment (spacer) in suppression and replacement constructs. The effects of various elements on *RHO*-BB expression were tested in these constructs. β-G int: human β-globin intron, *HGH* pA: human growth hormone poly-adenylation signal, CMVE: CMV enhancer, 3'UTR: 3'-UTR of *RHO* mRNA including poly-adenylation signals, WPRE: woodchuck hepatitis post-transcriptional regulatory element, E: conserved region E of the *Rho*-P (Supplemental Table 1), B: conserved region B of the *Rho* (Supplemental Table 1), m pA: minimal poly-adenylation signal. Restriction enzyme sites used for cloning are given. Numbers indicate molecular sizes in base pairs, and arrows indicate the direction of transcription.

Figure 2. Retinal EGFP expression from CMV and *Rho* promoter driven AAV constructs

Adult wild type mice were subretinally injected with 1 x 10^{10} vp/eye AAV-CMV-P-EGFP and AAV-*Rho*-P-EGFP. Two weeks post-injection, eyes were either fixed in 4% paraformaldehyde, cryosectioned (12 μm) and nuclei counterstained with DAPI or prepared for FACS analysis. Representative microscope images are shown from eyes injected with AAV-CMV-P-EGFP (A; n=3) and AAV-*Rho*-P-EGFP (C; n=3).

PSL: photoreceptor segment layer; ONL: outer nuclear layer; INL: inner nuclear layer. Scale bar: 25 μm. Other retinas (n=3) were dissociated with trypsin and retinal cells analyzed by FACS. Representative EGFP fluorescence histograms are given for both AAV-CMV-P-EGFP (B) and AAV-*Rho*-P-EGFP (D). Red arrows indicate the mean fluorescence levels of the green cell populations. EGFP-positive cells were sorted, RNA purified and RHO mRNA expression quantified by qRT-PCR (E). The mean of EGFP expression from the CMV promoter was taken as 100%. Error bars represent SD values, ***: $p<0.001$.

Figure 3. Retinal RHO mRNA expression from various AAV constructs

Adult wild type mice were subretinally injected with 1 x 10^{10} vp/eye AAV-*RHO*-BB constructs (BB8, BB9, BB10, BB13, BB24 and BB32; n=10 expect for BB32 where n=5) and *RHO* mRNA expression analyzed by qRT-PCR ten days post-injection. Light blue columns indicate *RHO* mRNA expression from AAV-transduced retinas. *RHO* mRNA expression level in RHO-M transgenic mice was used as control and taken as 100% (dark blue column). Error bars represent SD values, ***: $p<0.001$ (compared to RHO-M), ***: $p<0.001$ (compared to BB8), * and *** above the arrows indicate: $p<0.05$ (BB24 versus BB13) and $p<0.001$ (BB32 versus BB13).

Figure 4. Immunohistochemical analysis of RHO expression in AAV transduced retinas of wild type mice

Adult wild type mice were subretinally injected with 2 x 10^{9} vp/eye of AAV-CMV-P-EGFP (A and B; injection control), AAV-BB8 (C and D), AAV-BB13 (E and F) and AAV-BB24 (G and H); RHO-M mice (I and J) were used as positive control (n=4). AAV-BB8, AAV-BB13 and AAV-BB24 were supplemented with a 1/10 volume of

AAV-CMV-P-EGFP tracer. Two weeks post-injection, eyes were fixed in 4% paraformaldehyde, cryosectioned (12 μm) and immunocytochemistry using human RHO-specific primary and Cy3-conjugated secondary antibodies carried out; nuclei were counterstained with DAPI. A, C, E, G and I: Representative microscope images indicating RHO labelling (red). B, D, F, H and J: RHO (red), EGFP (green) and nuclear DAPI (blue) signals overlaid. PSL: photoreceptor segment layer (this layer is also marked by *); ONL: outer nuclear layer; INL: inner nuclear layer; GCL: ganglion cell layer; scale bar: 25 μm. Note that RHO and EGFP labels are not present in A and J, respectively.

Figure 5. Immunohistochemical analysis of RHO expression in AAV-transduced retinas of *Rho-/-* mice at six weeks post-injection

The right eyes of newborn *Rho-/-* mice were subretinally injected with 3.9 x 10^9 vp/eye of AAV-BB13 (C and D) and AAV-BB24 (E and F) both supplemented with a 1/10 volume of AAV-CMV-P-EGFP tracer, while the left eyes were un-injected (A and B; n=5). Six weeks post-injection, eyes were fixed in 4% paraformaldehyde, cryosectioned (12 μm) and immunocytochemistry using rho primary and Cy3-conjugated secondary antibodies carried out; nuclei were counterstained with DAPI. A, C and E: Representative microscope images indicate RHO labelling (red). B, D and F: RHO (red), EGFP (green) and nuclear DAPI (blue) signals overlaid. PSL: photoreceptor segment layer (this layer is also marked by *); ONL: outer nuclear layer; INL: inner nuclear layer; GCL: ganglion cell layer; scale bar: 25 μm. Note that RHO and EGFP labels are not present in A and B.

Figure 6. Immunohistochemical analysis of RHO expression in AAV-transduced retinas of *Rho-/-* mice at twelve weeks post-injection

The right eyes of newborn *Rho-/-* mice (n=5) were subretinally injected with 3.9 x 10^9 AAV-BB24 (BB24) supplemented with a 1/10 volume of AAV-CMV-P-EGFP tracer, (C and D) while the left eyes were un-injected (A and B). Twelve weeks post-injection, eyes were fixed in 4% paraformaldehyde, cryosectioned (12 μm) and immunocytochemistry using rhodopsin primary and Cy3-conjugated secondary antibodies carried out; nuclei were counterstained with DAPI. A and C: Representative microscope images indicate RHO labelling (red). B and D: RHO (red), EGFP (green) and nuclear DAPI (blue) signals overlaid. PSL: photoreceptor segment layer; ONL: outer nuclear layer; INL: inner nuclear layer; GCL: ganglion cell layer; scale bar: 25 μm. Note that RHO and EGFP labels are not present in A and B.

Figure 7. Rod-derived ERG of *Rho-/-* mice six weeks post-injection of AAV-BB24

The right eyes of newborn *Rho-/-* mice were subretinally injected with two doses of either 3.9 x 10^9 vp/eye (n=10) or 6.5 x 10^9 vp/eye (n=3) of AAV-BB24, including $1/10^{th}$ of AAV-EGFP tracer, while the left eyes were un-injected. Six weeks post-injection, mice were dark-adapted overnight and rod-isolated ERG responses recorded from both eyes; age-matched RHO-M mice were used as controls (n=8). A, C and E: Overlays of the ERG recordings (for the two AAV doses and RHO-M, respectively); blue and green lines represent recordings from un-injected and AAV-BB24 (BB24) injected eyes, respectively. B, D and F: mean ERG amplitudes. Blue and green columns represent values corresponding to un-injected and AAV-BB24 (BB24) injected eyes, respectively. Error bars represent SD values, ***: $p<0.001$, *: $p<0.05$. Note the different scales of the diagrams.

Figure 8. Comparison of rod-derived ERG of *Rho-/-* mice at six and twelve weeks following subretinal administration of AAV-BB24

The right eyes of newborn *Rho-/-* mice were subretinally injected with 3.9 x 10^9 vp/eye (n=12) of AAV-BB24 (including $1/10^{th}$ of AAV-EGFP tracer) while the left eyes remained un-injected. Rod-isolated ERGs were recorded at both six and twelve weeks post-injection in each mice; mice were dark-adapted overnight before analysis. b-wave amplitudes at six and twelve weeks are given for individual animals (blue). The mean of amplitudes are given in red. Error bars represent SD values, ***: $p<0.001$.

Figure 9. Ultrastructural analysis of *Rho-/-* retinas transduced by AAV-BB24

The right eyes of newborn *Rho-/-* mice (B) were subretinally injected with AAV-BB24 (including 1/10th of AAV-EGFP tracer) while the left eyes were un-injected (A). Six weeks post-injection, eyes were fixed and whole mounted. Transduced (3) and un-transduced (2) areas of the retinas were identified by the EGFP fluorescence and representative areas were excised. Control samples from un-injected (1) eyes were also prepared. The excised retinal samples were postfixed and further processed for transmission electron microscopy (TEM). Semi- and ultra-thin sections were analysed either by light microscopy (C, E, G) or TEM (D, E, F) for morphological characteristics. Expression of AAV-BB24 results in rod photoreceptor outer segments (ROS) reaching to the retinal pigment epithelium (RPE). In contrast in un-injected and un-transduced retinas only short truncated ROS (*) extend from the apical membrane of the rod photoreceptor inner segment (RIS). PSL: photoreceptor segment

layer, ONL: outer nuclear layer, INL: inner nuclear layer, GCL: ganglion cell layer, red arrows: extracellular space between PSL and RPE. Scale bars: 1 mm (A and B), 10 μm (C, E and G), 2.5 μm (D, F and H).

Figure 10. Photoreceptor rescue in *Rho-/-* retinas transduced by AAV-BB24

Transmisson electron micrographs of longitudinal ultra-thin sections through parts of rod photoreceptors of an un-transduced (A) and transduced retinas (B, C, D). A: In an un-transduced rod photoreceptor a ciliary process (= connecting cilium; CC) arises from the rod photoreceptor inner segment (RIS) differentiating into a truncated outer segment (*) without any disks at its tip. A red arrow indicates the wide distance of the extracellular space between the photoreceptor segment and the retinal pigment epithelium (RPE). B: In a transduced and rescued rod photoreceptor RIS, CC and outer segment (ROS) show the morphologic characteristics of wildtype photoreceptors. C: The plasma membrane of the ROS tip of a rescued rod photoreceptor touches the membrane of RPE cells (red arrowheads). D: Correctly formed membrane disks in the ROS of a transduced and rescued rod photoreceptor. Scale bars: 500 nm (A, B and C); 100 nm (D).

Supplementary Figure 1. Cone-isolated ERG of *Rho-/-* mice six weeks post-injection of AAV-BB24

The right eyes of newborn *Rho-/-* mice were subretinally injected with 3.9 x 10^9 vp/eye (n=10) of AAV-BB24 (including $1/10^{th}$ of AAV-EGFP tracer) or PBS alone (n=4) while the left eyes were un-injected. Six weeks post-injection, mice were dark-adapted overnight and cone-isolated ERG responses (b-wave amplitudes) recorded from both eyes. Mean ERG amplitudes are given for un-injected control (light blue),

AAV-BB24 (BB24, green) and PBS (dark blue) injected eyes. Error bars represent SD values, ***: $p<0.001$. Note that b-wave amplitudes of AAV-BB24 and PBS injected eyes did not differ significantly ($p=0.54$).

Supplemental Figure 2. Phagocytosis of outer segements in Rho-/- retinas transduced by AAV-BB24

Transmission electron micrograph of a longitudinal ultra-thin section demonstrates the phagocytotic incorporation of shed rod photoreceptor outer segement disc stacks (pROS) by the retinal pigment epithelium (RPE) after AAV-BB24 transduction. ROS: rod photoreceptor outer segment tip. Scale bar: 500 nm.

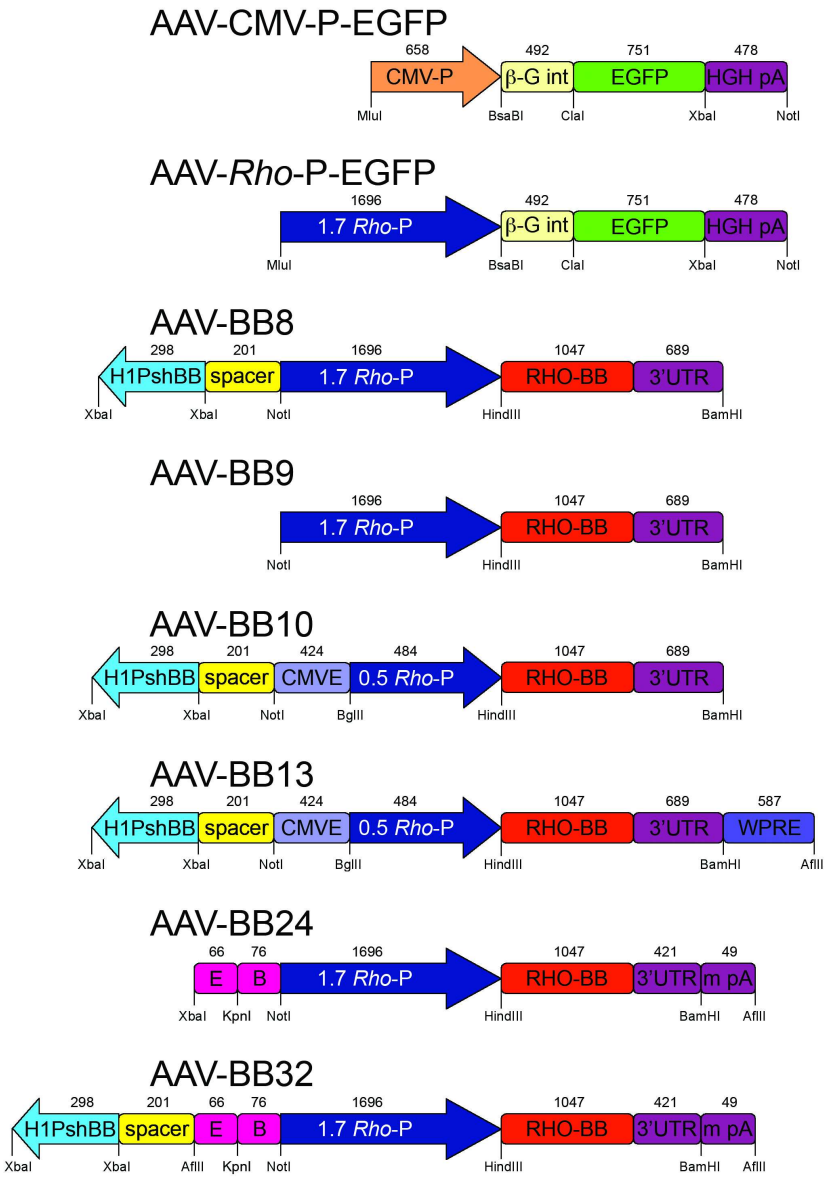

175x251mm (300 x 300 DPI)

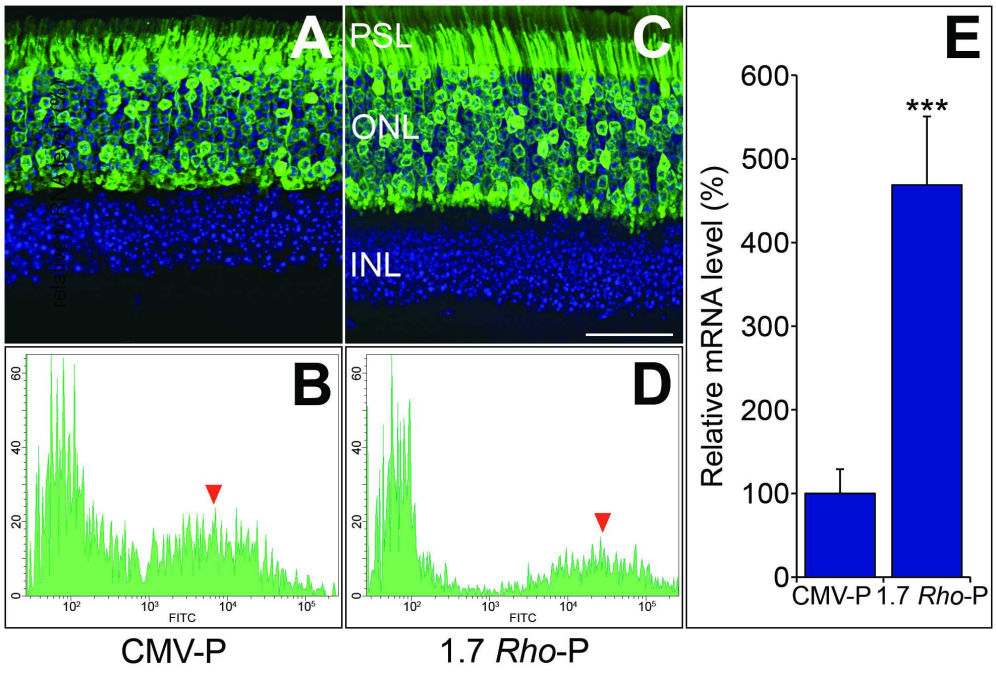

167x113mm (300 x 300 DPI)

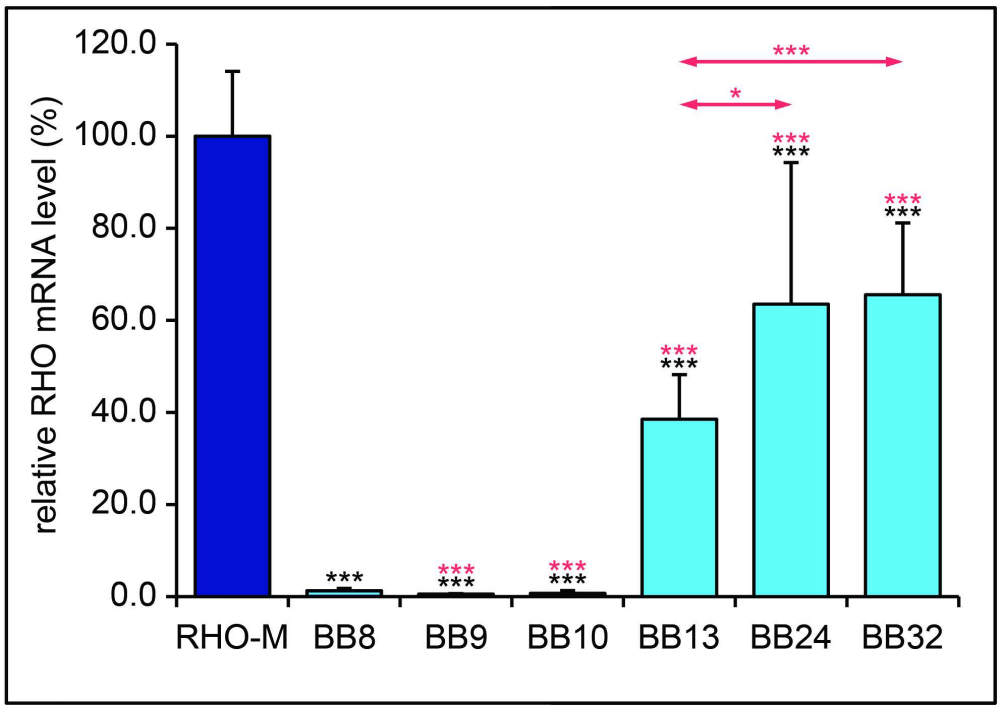

167x118mm (300 x 300 DPI)

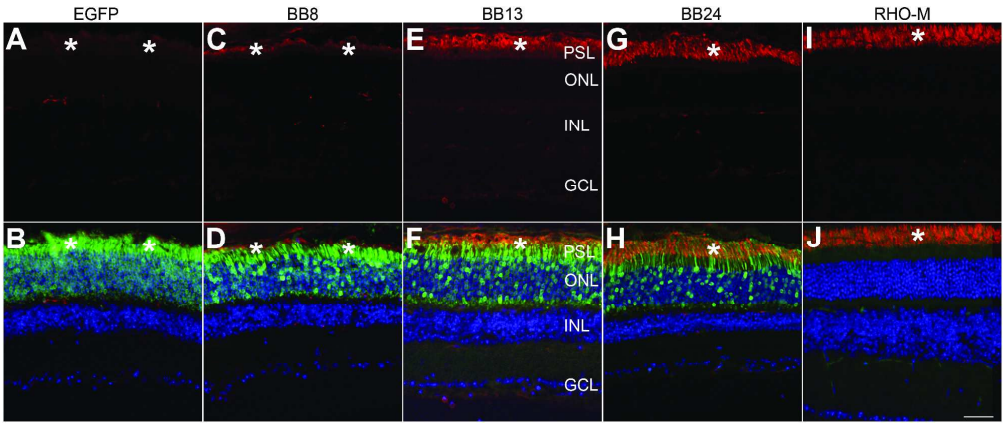

337x140mm (300 x 300 DPI)

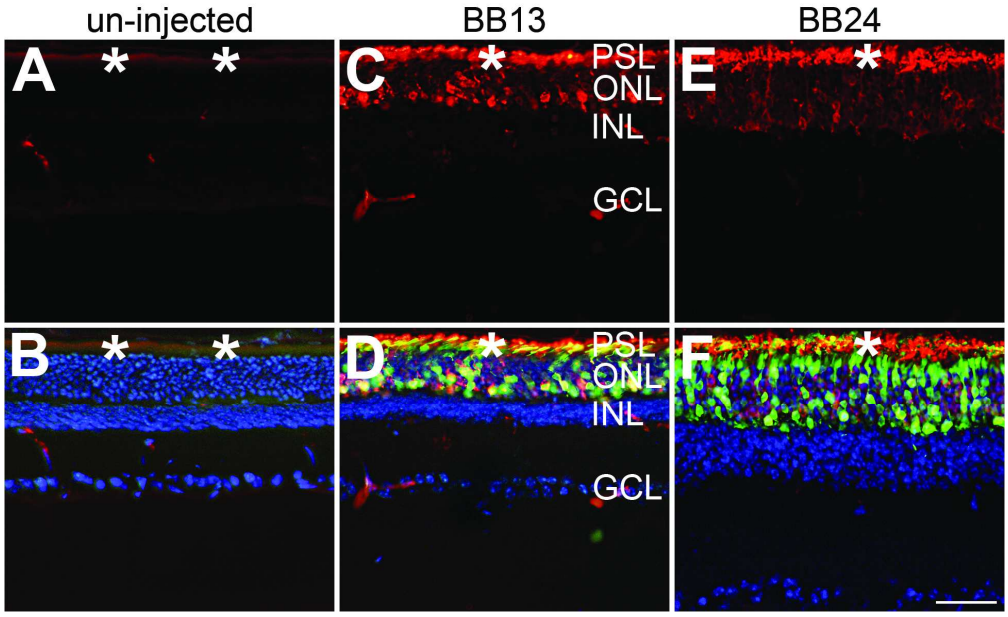

164x102mm (300 x 300 DPI)

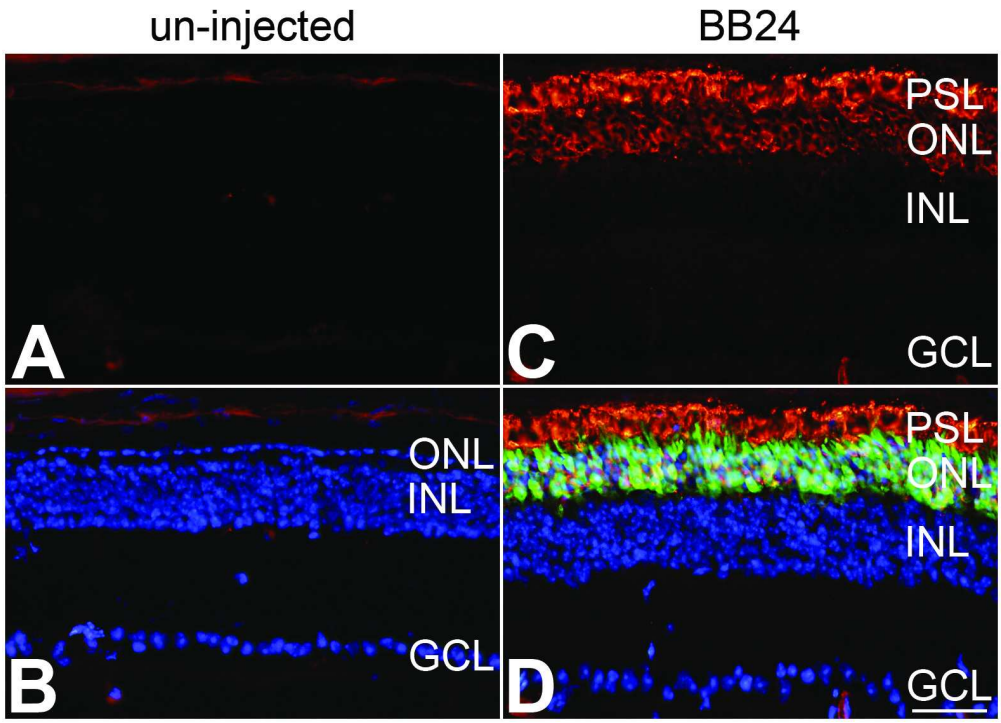

66x48mm (600 x 600 DPI)

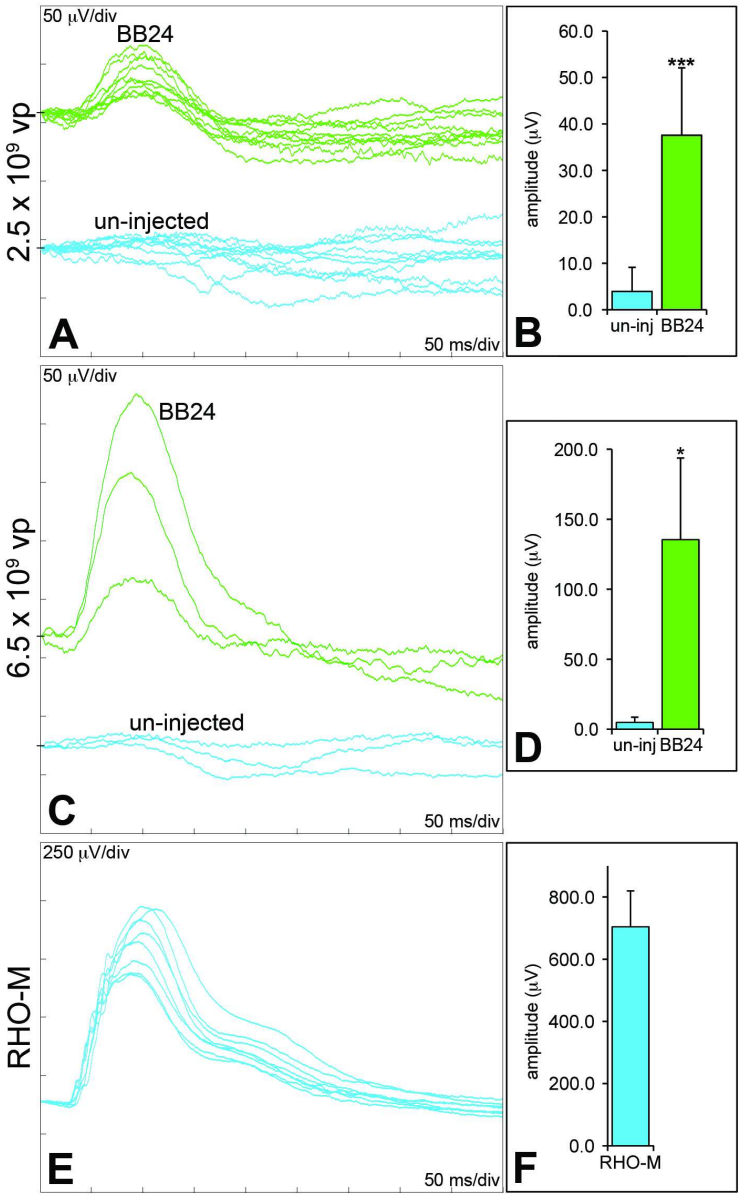

118x193mm (300 x 300 DPI)

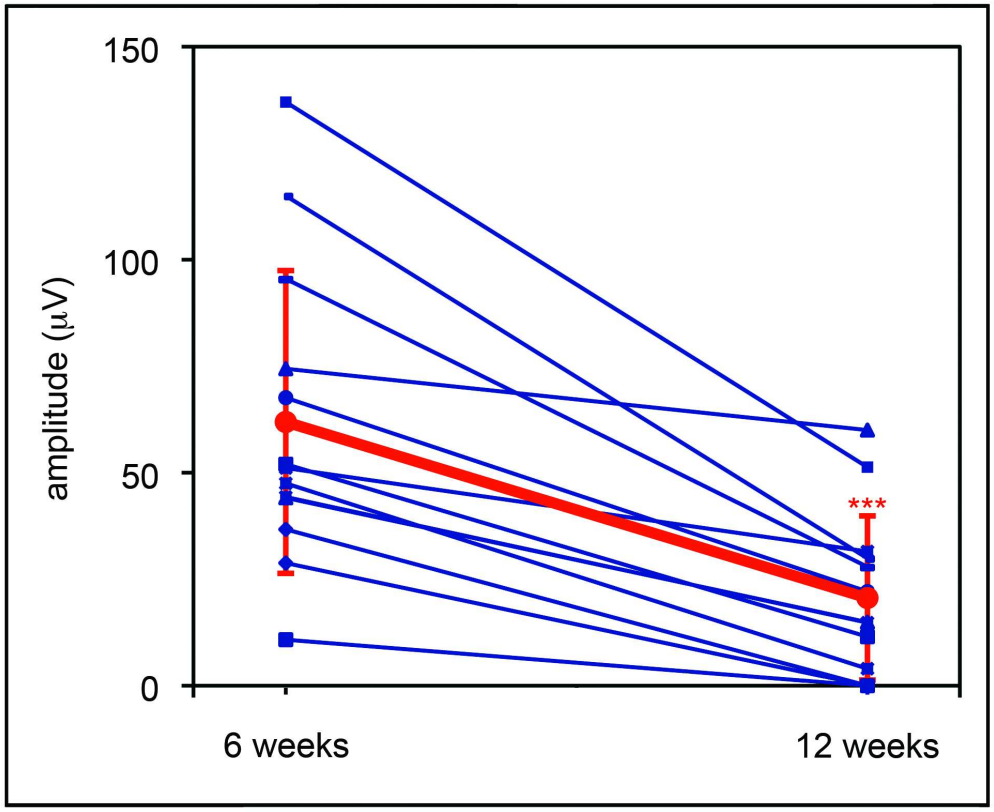

81x67mm (600 x 600 DPI)

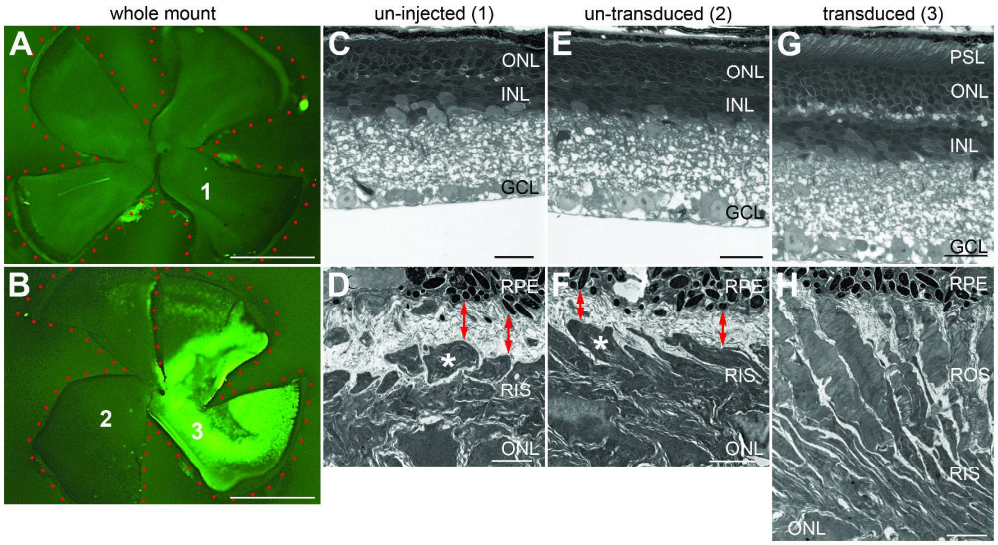

302x165mm (300 x 300 DPI)

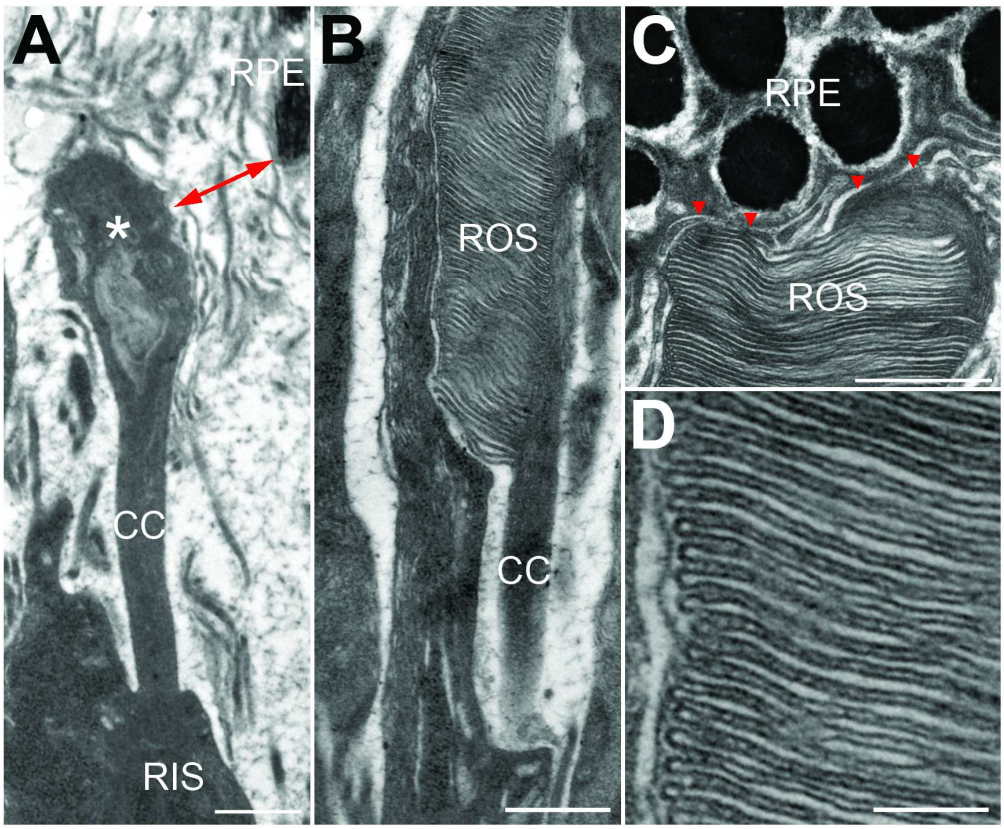

146x120mm (300 x 300 DPI)

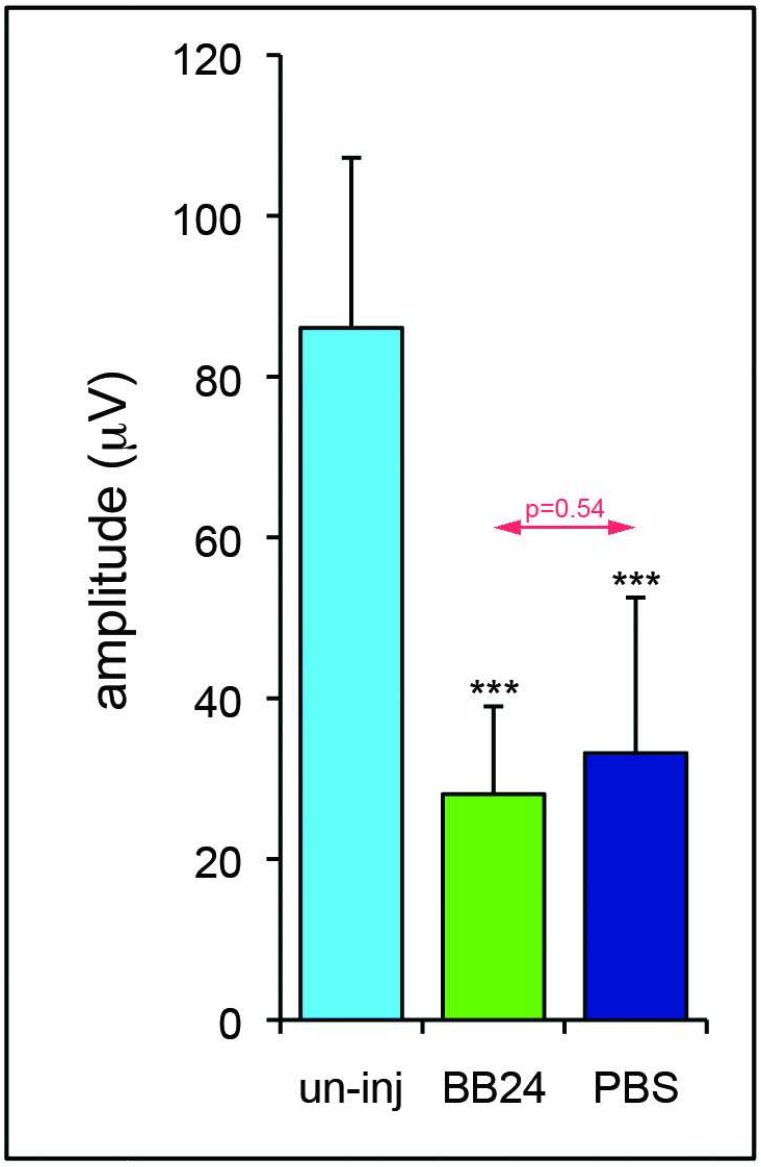

32x48mm (600 x 600 DPI)

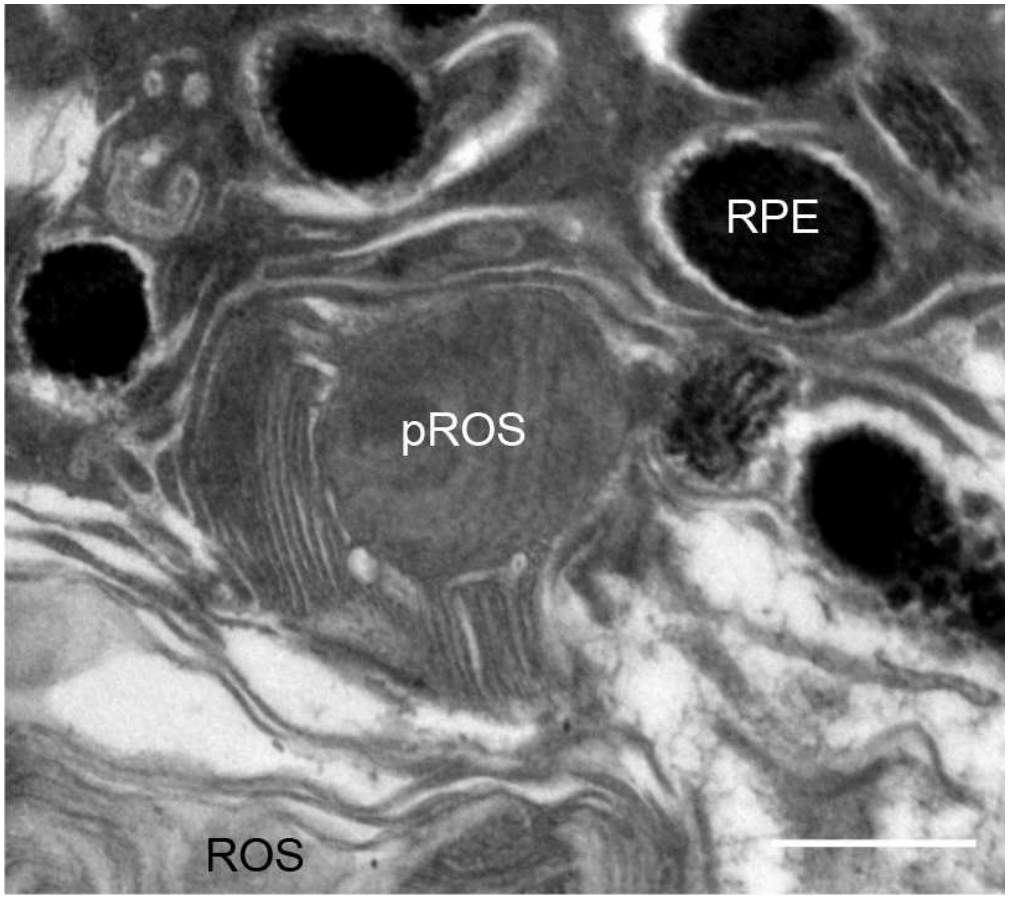

68x60mm (300 x 300 DPI)

Supplemental Table 1. Conserved Promoter Elements

Element	Accession number	Position	Predicted transcription factor binding sites	Sequence 5'-3'
E	NT_005612	35742513 - 35742578	CRX (-) & NRL (+)	TTTCTGCAGCGGGGATTAATATGATTATGAACACCCCCAATCTCCCAGATGCTGATTCAGCCAGGA
B	AC142099.3	24955-24880	CRX (+)	TCCCTAATCCTCCATTC

Footnote

CRX: Cone-Rod homeobox-containing transcription factor, NRL: Neural Retinal basic Leucine zipper factor.